

Status of MAGIC-II

A. Moralejo

Institut de Física d'Altes Energies, Bellaterra, Barcelona 08193, Spain
for the MAGIC collaboration

A status report of the second phase of the MAGIC ground-based gamma-ray facility (as of October 2009) is presented. MAGIC became recently a stereoscopic Cherenkov observatory with the inauguration of its second telescope, MAGIC-II, which is currently approaching the end of its commissioning stage.

1. INTRODUCTION

MAGIC, a gamma-ray imaging atmospheric Cherenkov facility [1] composed up to now of a single telescope, has become a stereoscopic system with the inclusion of a second telescope, MAGIC-II. MAGIC is located on the Canary island of La Palma (28.8° N, 17.9° W), and operates in the very high energy spectral band (photon energies above 30 GeV). MAGIC-II saw its first light in Spring 2009, and is now approaching the end of its commissioning phase. Whereas from the mechanical point of view MAGIC-II is essentially a clone of the first telescope, it features significant improvements in other aspects, like a more finely pixelized camera and a lower-cost, more compact readout system.

2. THE MIRROR DISH

The mirror dish of MAGIC-II is a tessellated paraboloid of 17 m focal length and $f/D=1$. Each of the 247 square tiles is a spherical mirror with a surface of 1 m², mounted on two motors which allow to adjust its orientation to ensure that the parabolic shape is maintained, despite the sagging of the telescope structure, for different orientations of the instrument. The reflecting surfaces of the inner 143 mirror tiles [2] are diamond-milled aluminum plates (the same technology used in MAGIC-I), whereas the outer 104 are equipped with thin aluminum-coated glass sheets [3]; in both types of mirrors the needed mechanical stiffness is provided by an underlying aluminum honeycomb structure. The optical properties of MAGIC-II are similar to those of the first telescope. About 66% of the light from a point source is contained within the area of one camera pixel (see fig. 2). The good optical quality of the mirror dish is confirmed by the analysis of muon ring images (a typical one is shown in fig. 3).

3. CAMERA AND DATA ACQUISITION

The camera of MAGIC-II (see left pad of fig. 3) is composed of 1039 photomultiplier tubes of 0.1°Ø, for

a total field of view of 3.5°. The innermost 559 pixels take part in the trigger (covering a 70% larger area than in M-I).

The signals from the 1039 PMTs on the MAGIC-II camera are converted into analog optical pulses which are sent to the control building 80 m away via optical fibres, where they are converted back into electronic pulses and then split to provide the input for the trigger and the signal sampling systems. The readout system of MAGIC-II is based on version 2 of the Domino Ring Sampler chip (DRS2). The chip samples the input signals analogically at 2 Gsample/s using an array of 1024 capacitors (so-called cells). In case of a trigger, the sampling is stopped and the data are digitized with a 12-bit resolution ADC at 40 MHz. Data management is based on a digital board called PULSAR that handles up to 80 analog channels. 80 samples (one every 0.5 ns) are recorded per pixel for each triggered event. [4].

The response of DRS2 chip is not linear, and amplitudes have to be corrected as the first step in the processing of the data. A dedicated calibration of every capacitor in every channel ($> 10^6$ instances) is performed once per night for this purpose (see fig. 1). Saturation of the signal occurs at about 900 photoelectrons.

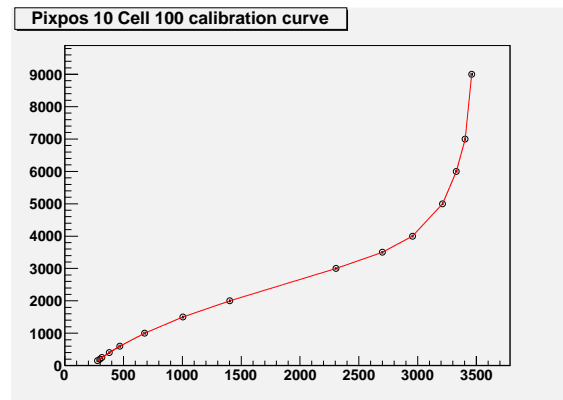


Figure 1: Typical linearity calibration curve of a cell in a DRS2 channel. The input signal (in units of 0.1 mV) is in the vertical axis, while the horizontal one shows the output value in ADC counts.

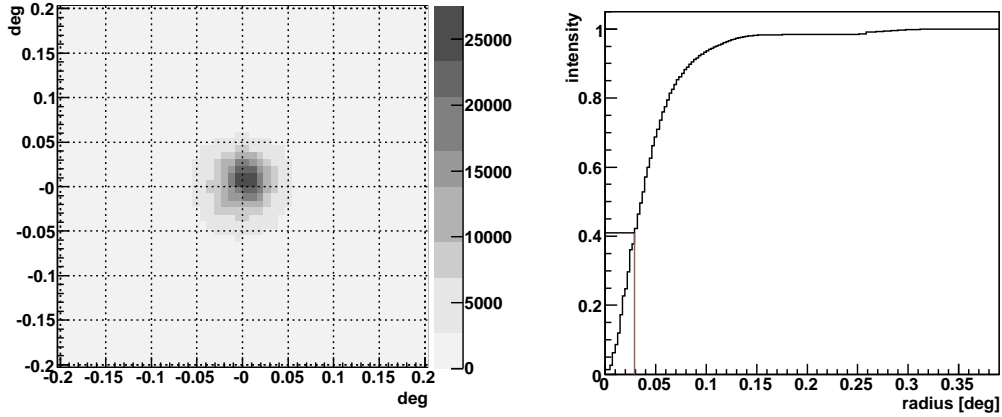


Figure 2: Optical point spread function of MAGIC-II. The radius of the camera pixels is 0.05° . 66% of the light from a point source impinging parallel to the optical axis of the telescope is collected within one pixel.

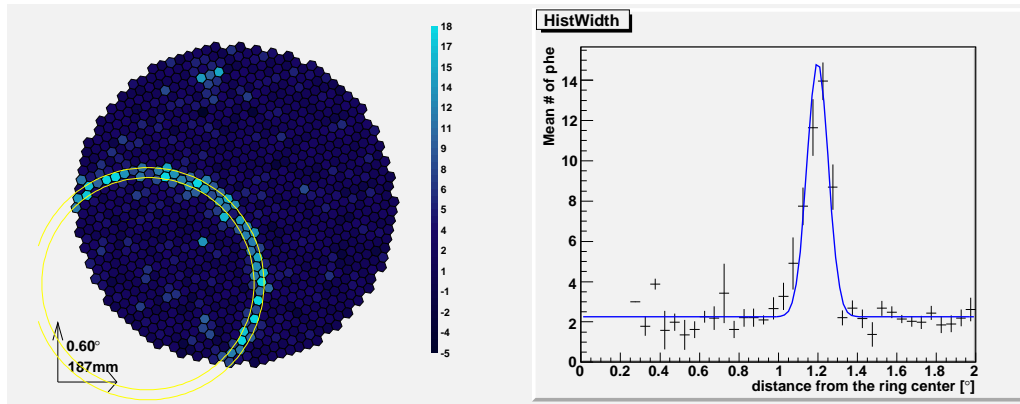


Figure 3: A muon ring recorded in September 2009. On the right pad, the transversal light profile of the ring. The width of the ring confirms the good optical properties of the MAGIC-II mirror dish.

Occasionally, data are contaminated by sharp regular spikes (in isolated cells) which can be identified and have to be cured by software, through interpolation of the values in neighboring cells, as part of the signal extraction process. This effect is rare, affecting just about 3% of the measurements, and does not spoil the data in a significant manner.

A cell-dependent correction of the signal timing is also needed. In figure 4 the average reconstructed arrival time of laser calibration pulses (fast flashes which illuminate uniformly the whole camera) is shown for a given channel as a function of the number of the first DRS cell written out in each event. The observed modulation is due to the non-uniform speed of the “Domino wave” that determines which cell is sampling the input signal at a given time. The curve shown in fig. 4 is characteristic of each channel and stable in time. One such curve per channel is used for the offline correction of the signal arrival times.

4. FIRST OBSERVATIONS

Stereoscopic observations of the Crab Nebula are being performed with the two MAGIC telescopes since September 2009. The stereo trigger system (with orientation-dependent adjustable signal delays) is in operation since November, but the results shown below correspond to earlier observations, carried out in “software stereo” mode (with each telescope recording events independently, followed by offline matching of the events).

4.1. Data analysis

After a conventional two-level image cleaning procedure, a simple geometrical reconstruction has been applied to obtain an estimate of the shower axis geometry (direction and impact point) as the intersection

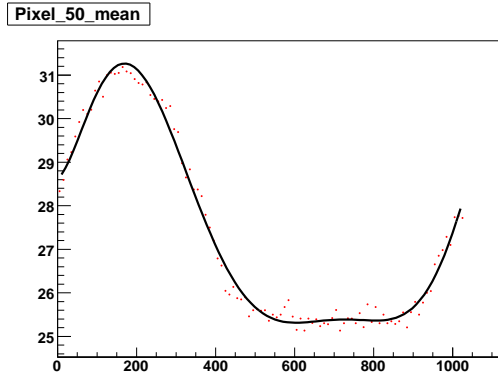


Figure 4: Dependence of the arrival time (y-axis, units: 0.5 ns) of laser calibration pulses in a certain channel with the number of the first DRS2 cell written out (shown in the x-axis). This behaviour is characteristic of the DRS2 chip, and can be fully corrected offline in order to get the right pulse arrival times in every pixel.

of two planes – one per telescope¹. The background suppression relies in the *Random Forest* algorithm [6], fed with image parameters from the individual telescopes and also with shower parameters obtained from the stereoscopic reconstruction (like the shower impact point and the height of the shower maximum). The *Random Forest* is trained on a sample of Monte Carlo gammas and real background events (from observations of an empty sky region), and then applied to the Crab Nebula data in order to obtain for each event a single value, dubbed *hadronness*, which will be used as cut parameter for background rejection.

4.2. Preliminary results

A map of reconstructed event directions (in camera coordinates) with respect to the Crab Nebula is shown in fig. 5 for 87 minutes of *wobble* observations (i.e. with the telescope pointing 0.4° away from the source direction). The corresponding angular distribution of events around the source is presented in fig. 6. No offline pointing correction has been applied. The selected event sample includes only events with at least 400 photoelectrons in each of the telescopes, resulting in a peak gamma energy $\simeq 400$ GeV. It is therefore a high energy sample, very much above the energy threshold of the instrument (of around 50 GeV), but roughly where the best integral flux sensitivity is expected.

¹More sophisticated methods, involving the use of the pixel timing information, which proved useful in the analysis of single telescope data [5], are being investigated, and preliminary results are promising.

In terms of flux sensitivity, the observed performance of the stereoscopic system is already clearly superior to that of MAGIC-I in standalone observations, and is approaching the Monte Carlo expectations. Precise tuning of the Monte Carlo simulation to the characteristics of MAGIC-II is ongoing, and is expected to improve further the performance of the system.

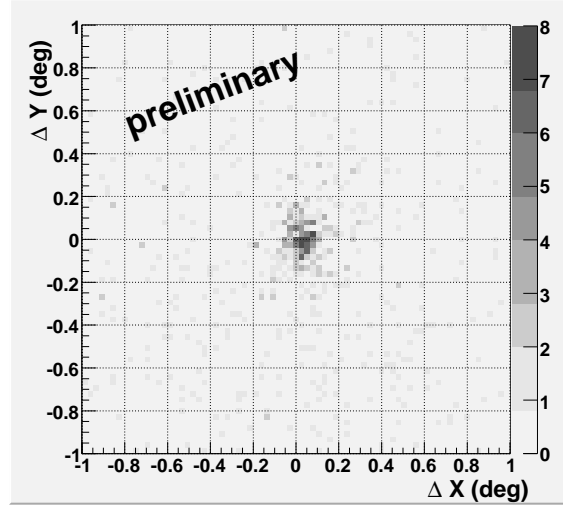


Figure 5: Distribution of reconstructed event directions in camera coordinates, with (0, 0) corresponding to the position of the Crab Nebula. The event sample is the same of fig. 6

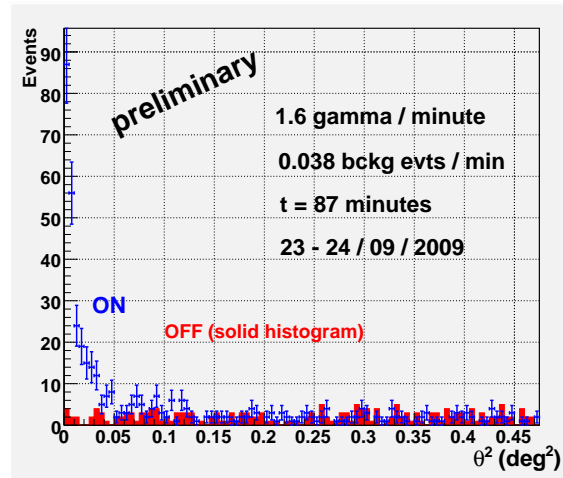


Figure 6: Angular distribution of excess events around the Crab Nebula (θ^2 is the squared angular distance between the reconstructed event direction and the nominal source direction). The event sample here displayed (see text) corresponds to a peak gamma energy of around 400 GeV.

5. CONCLUSIONS

The second telescope of the MAGIC ground-based gamma-ray observatory is already operational, and is performing stereoscopic observations since September. Preliminary results of the observations of the Crab Nebula show already a very significant boost in performance with respect to the standalone MAGIC-I telescope, particularly in terms of flux sensitivity. Work is ongoing in polishing the analysis methods and improving the agreement of the Monte Carlo simulation with data, both of them aspects in which there is still some room for improvement.

References

- [1] J. Cortina et al, “Technical Performance of the MAGIC Telescopes”, Proc. of the 31st ICRC, Lódź, 2009
- [2] M. Doro et al, “The reflective surface of the MAGIC telescope”, NIM A, Volume 595, Issue 1, 2008
- [3] G. Pareschi et al, “Glass Mirrors by cold slumping to cover 100 m² of the MAGIC II Cherenkov telescope reflecting surface”, Proc. of the SPIE, Volume 7018, 2008
- [4] D. Tescaro et al, “The readout system of the MAGIC-II Cherenkov Telescope”, Proc. of the 31st ICRC, Lódź, 2009
- [5] E. Aliu et al, “Improving the performance of the single-dish Cherenkov telescope MAGIC through the use of signal timing”, Astropart. Phys. 30, 2009
- [6] J. Albert et al, “Implementation of the Random Forest Method for the Imaging Atmospheric Cherenkov Telescope MAGIC”, Nucl. Instr. Meth. A 588, 2008